Studies of Carbonaceous Materials using Raman Spectroscopy

by

Cameron Smith

A thesis submitted to the faculty of The University of Mississippi in partial fulfillment of the requirements of the Sally McDonnell Barksdale Honors College

Oxford, Mississippi

May 2018

Approved by:

_____

Advisor: Professor Nathan Hammer

_____

Reader: Professor Wei-Yin Chen

_____

Reader: Chair Gregory Tschumper

Abstract

CAMERON L. SMITH: Studies of Carbonaceous Materials using Raman Spectroscopy

(Under the guidance of Dr. Nathan Hammer)

Various carbonaceous materials including graphene, treated biochar, and C_{60} were studied using Raman spectroscopy with particular attention given to the treatment process and the Raman enhancement methods. Such studies that focus on the treatment process are useful in determining the extent to which the species was affected via shifts in the Raman peaks. Previous collaborations have proven successful when multiple samples were studied and analyzed. The attempt to create a novel Raman enhancement technique via combination of two previously recorded techniques was ultimately unsuccessful but further work is necessary.

Table of Contents

List of Figures

List of Tables

List of Abbreviations

C_{60}	Carbon 60 (Buckminsterfullerene)
SERS	Surface Enhanced Raman Spectroscopy
TERS	Tip Enhanced Raman Spectrocopy
RUNS	Raman Under Liquid Nitrogen Spectroscopy
SERSUN	Surface Enhanced Raman Spectroscopy Under Liquid Nitrogen
YAG	Yttrium Aluminum Garnet
VDC	Vapor Deposition Chamber
CCD	Charge Coupled Device
GO	Graphene Oxide
TEPA	Tetraethylenepentamine
CO_2	Carbon Dioxide
π	pi (bond)
TiO_2	Titanium Dioxide
GO-TiO_2	Graphene Oxide – Titanium Dioxide
EDC	1-Ethyl-3-(3-Dimethylaminopropyl)Carbodiimide
VDC	Vapor Deposition Chamber

Chapter 1 Introduction

Spectroscopy is the study of light and matter interactions. For researchers, the interesting part of this interaction is that light usually undergoes a change in wavelength and hence energy once a photon comes in contact with matter. This change in energy of the photons which struck the matter marks a change in energy of the surrounding as shown in Figure 1. Most often this change in energy is noted by a change in energy of the matter which the photon contacted. Given that energy levels in matter consist of translational, rotational, vibrational, and electronic energy states, the matter may undergo many discrete interactions depending on the wavelength and intensity of the incident light.

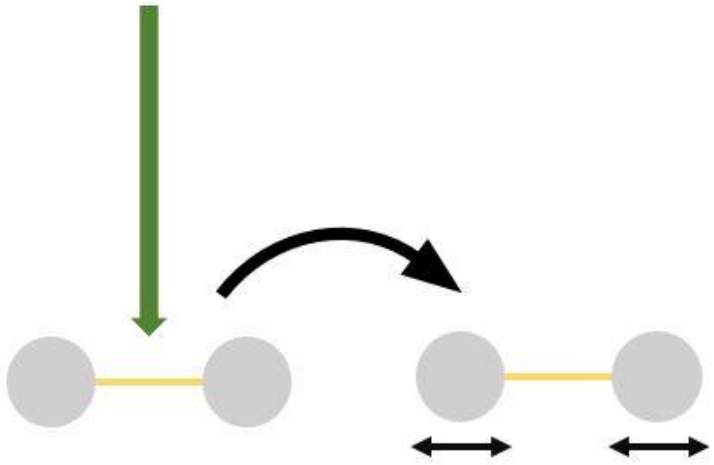

Figure 1 Excitation: The above image represents the vibrational excitation of a molecule when struck by a photon of a particular wavelengths. The particular vibration is a stretching motion.

The energy states of matter on a macroscopic level appear to be continuous given the number of molecules present but quantum mechanics has shown that energy states are in fact discrete and quantized; meaning that each energy level transition is experimentally measurable. Spectroscopy uses this fundamental characteristic to study how light and matter interact.

1.1 Raman Spectroscopy

Although many have questioned why the sky and ocean are blue, it was not until the 1920's with the advent of the Raman Effect[1] that the scientific reasoning behind such phenomenon became apparent. Although Sir C.V. Raman would not live to see his theory come to full experimental fruition with the surge in advanced laser technology,[2] he had in effect laid the mental groundwork for a future field of research that would be both extensive and encompassing.

Electromagnetic radiation exists on a spectrum that ranges from long radio waves with the longest wavelength to gamma rays with the shortest wavelength. Although commonly divided into categories, the differences between categories are purely arbitrary with respect to any properties save wavelength, energy, and frequency which are all directly related and are in fact equivalent measurements of light. For Raman spectroscopy to be useful, a change in the polarizability of the molecule under study must occur.[3] In order for this to occur, incident light must possess enough energy to excite this transition but not so powerful as to destroy the sample's chemical structure as demonstrated in

Figure 2. Generally, light in the visible and near-infrared regions of the light spectrum are used in the form of monochromatic radiation such as lasers.

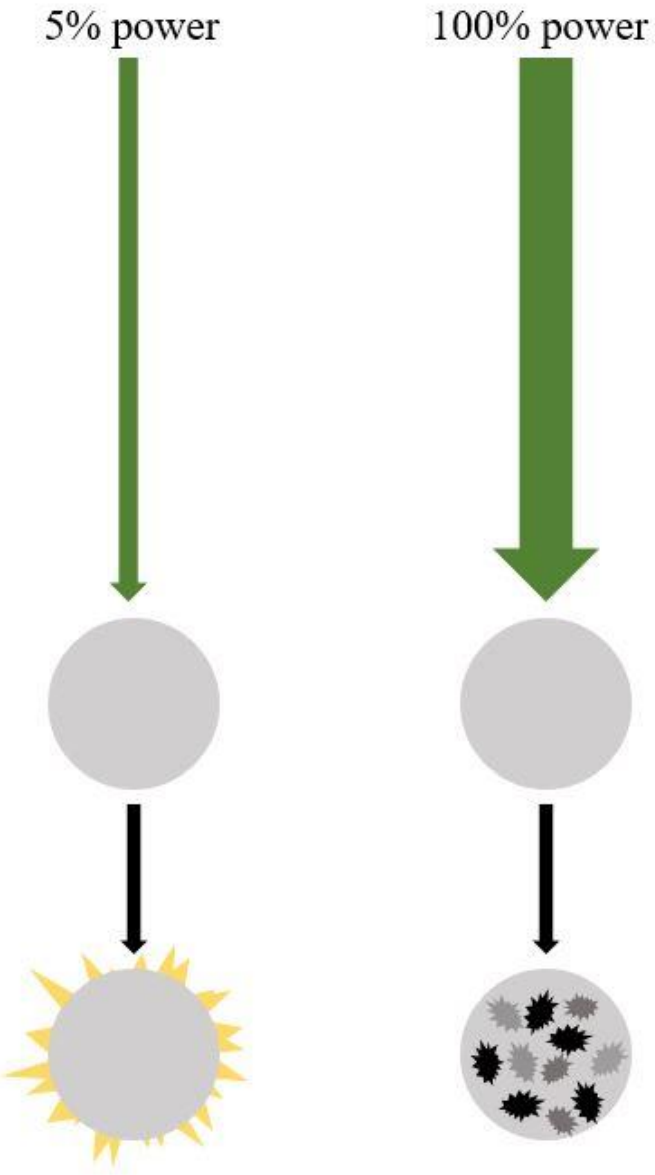

Figure 2 Laser Power: Given that the carbonaceous molecules under study possess such a low flash point temperature,[4] it is possible to leave burn residue on the sample. This will certainly destroy the chemical structure of the sample and be unrepresentative of the whole.

Raman spectroscopy is based on the scattering of incident light as shown in Figure 3.[28] This scattering can either be an inelastic (of varying energy from the incident light) or elastic (of the same energy as the incident light) collision. Elastic scattering, commonly referred to as Rayleigh scattering, is the most common form of scattering; it is approximately six orders of magnitude more likely to occur than Stokes scattering. Inelastic scattering can be divided into two opposite categories: Stokes and Anti-Stokes. At ambient temperatures or below, most of the studied samples held vibrational energy levels in the ground state. As such, Stokes was the more common of the two inelastic scattering categories because the samples were excited from the ground state vibrational level to a virtual state and relaxed to a slightly higher vibrational state than the ground state but below the virtual state. At higher temperatures, the vibrational energy of the sample increase. As such, the intensity of Anti-Stokes peaks will increase because the samples are excited from an above ground state vibrational level to a virtual state and relaxed to the ground vibrational state. In essence, a scattered radiation can either be higher, lower, or the same energy as the incident radiation.

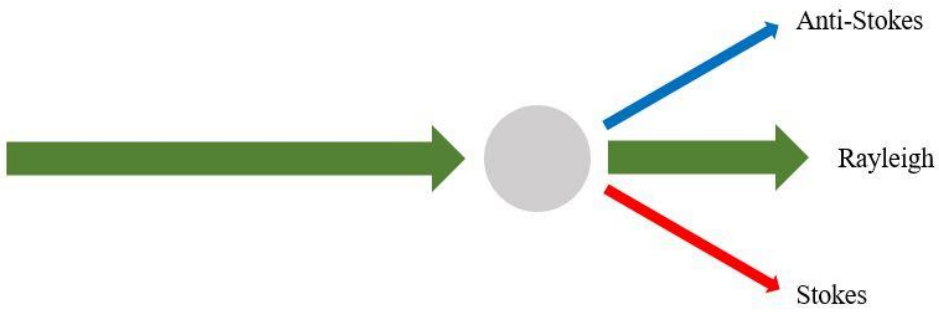

Figure 3 Raman Scattering: Once light interacts with a molecule, the scattered light is restricted to three possible categories: higher, lower, or same energy. Anti-Stokes is the highest energy, Rayleigh is no change in energy, and Stokes is the lowest energy.

When noting the specific peaks in a Raman spectrum, it is paramount that a spectroscopist be able to note the structural and chemical identity of the peak. Generally, the x-axis of a graph is labeled in Raman shift with units of cm^{-1}, which signify the energy of the scattered Raman light; the y-axis is in units of light intensity which is arbitrary save when comparing normalized peaks in a single measurement of a sample. While understanding the structural and chemical information of the Raman active modes is necessary, estimating the amount of a species active for that mode is also necessary. The estimation signifies the amount of a species that has a certain phase or bonding structure. Two methods can be used as relative estimates between related species: absolute maxima peak intensity and integrated area under a peak. While the integrated area under the peak is a more correct and accurate form of estimation, absolute maxima of peaks can be compared. The intensities will often be denoted as a I_X/I_Y ratio for peaks denoted X and Y respectively. It should also be noted that the absolute peak intensity is a quantitative measure of the molecules vibrating at the median value for that frequency if a Gaussian curve is approximated.

1.1.1 Principle of Raman Spectroscopy

As previously mentioned, Raman spectroscopy is characterized by the scattering of a photon by a molecule. This is commonly referred to as the Raman effect[5] after its discoverer C. V. Raman.[6] Scattering as illustrated in Figure 3 illustrates the fundamental physical effects that occurs when light scatters. Classically, the Raman effect can be described by the polarizability of a molecule. Given that equation (1) represents the induced dipole moment of a molecule:

$$\mu_{ind} = \alpha E \quad (1)$$

It is clear that the polarizability factor of the molecule, α, when in the presence of an applied electric field, E, will induce a dipole moment, μ_{ind}. Since light is composed of two perpendicular oscillating fields of electric and magnetic potential, the electric field when in close proximity will have an effect on the molecular electron cloud. It is this distortion of the electron cloud of the molecule and its atoms that is of interest to Raman spectroscopists. Therefore, it can be said that a change in the polarizability of a molecule is necessary for the molecule to have Raman active vibrational modes such as in Table 1.

1.1.2 Application of Raman Spectroscopy

What began as a relatively simplistic study of natural phenomenon[7] by modern scientific standards has blossomed into a wide-reaching field. From clinical application with hand-held spectrometers[8] to temperature-controlled biochemical studies,[9] Raman spectroscopists have entered nearly every field of science in which quick, non-invasive, non-hazardous, and time effective measurements of chemical structure and composition are needed. From method enhancements such as Surface Enhanced Raman Spectroscopy[10] to Tip Enahnced Raman Spectrocopy,[11] modern advances in technique have made the characterization of previously unstudied species possible. As will be discussed in following pages, a combination of two previously studies techniques, Raman Under Nitrogen Spectroscopy[12] and SERS, was attempted. RUNS involves submersing the sample of interest under a layer of liquid nitrogen to avoid sample degradation and oxidation, which is represented in Figure 4.[13] SERS is defined by the excitation of

localized surface plasmon resonances on nanostructured surfaces or nanoparticles via a thin coating of various metals films in physical contact with a vapor deposited sample layer.[14] Both enhancements methods are theorized to provide enhancements to resolution many orders of magnitude in size. Such a novel arrangement has not been attempted and published in literature. As such, the application of such method is largely unknown.

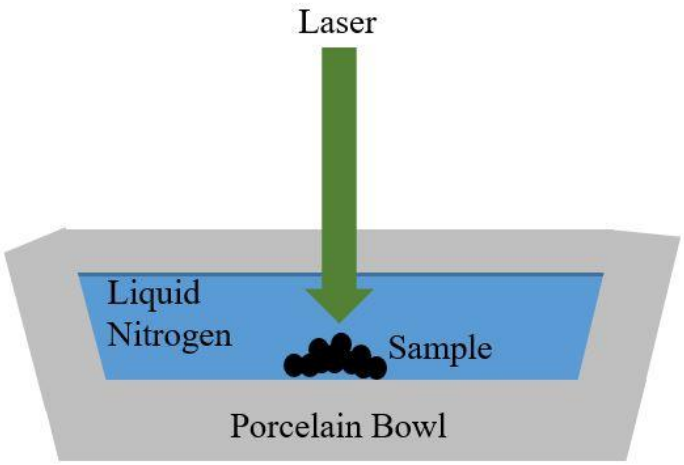

Figure 4 Raman Under Nitrogen: The sample is submerged under a layer of liquid nitrogen in the hollow of a porcelain bowl. Porcelain was chosen to avoid cracking the equipment from the low temperatures.

1.1.3 Instrumentation of Raman Spectroscopy

For all experimental data collected, a Horiba LabRAM HR Evolution Raman Spectrometer was used with primarily a green YAG 532 nm laser as depicted in Figures 1 through 5, although certain samples required a red-orange He-Ne 633 nm laser of lower energy to reduce fluorescence. The detector was a CCD camera. The most commonly used grating was 600 gr/mm with 1800 gr/mm used on rare occasions. The objective lens used was primarily a 100x zoom or on occasion 10x zoom. The power of the laser was

varied from approximately 6.2 mW at full power to 0.3 mW at 5% power for the 532 nm YAG laser.

Chapter 2 Samples

2.1 Graphene

Unintentionally created for centuries by the use of graphite pencils, graphene has been the focus of much scientific research since its isolation in 2004 by Andre Geim and Konstantin Novoselov at the University of Manchester[15] using the scotch tape method of mechanical exfoliation. Structurally, pristine graphene is composed of sp^2 bonded carbon atoms in a two-dimensional lattice; it is similar in bonding structure to that of chicken wire given its hexagonal pattern. Although it was studied decades before on metal surfaces using electron microscopes,[16] only after its physical isolation from a substrate was it brought into the scientific spotlight. Given its incredible properties of strength,[17] conductivity,[18] and optical activity,[19] graphene has become a candidate for many real-life applications that extend into nearly every field of engineering.

2.2 Biochar and Doped Graphene

Initially, studying amine functionalized biochar and doped graphene began as a collaboration project. Two separate collaborations were eventually established with Dr. Wei-Yin Chen and Dr. Sasan Nouranian of the Chemical Engineering department at the

University of Mississippi. The emphasis of the collaborations was to study the effects of treatment and doping using various experimental parameters and methods on biochar and graphene. The experimental design and sample preparation were sourced in the labs of Dr. Nouranian and Dr. Chen for their respective projects.

Doping samples has been proven many times to change the physical properties of carbonaceous materials.[20] The particular interests of doping the biochar and graphene were to capture CO_2, Ni(II), and organic molecules via ligand bonding to the graphene substrate, various ultrasound, urea, and phosphoric acid level treatments to the biochar, and graphene sheets on photocatalytic species such as TiO_2.

2.3 C_{60}

Having been studied and isolated before graphene,[21] C_{60} has been extensively studied and researched for decades. Under the advice from Dr. Bob Compton previously of the University of Tennessee at Knoxville, a new independent project began. The emphasis of this project was to combine two previously studied Raman enhancement methods, SERS and RUNS, into a novel technique tentatively named SERSUN. Given the lack of published work for the novel method, this would prove to be the most difficult work to date.

Chapter 3 Methods

3.1 Preparation

One of the advantages of using Raman spectroscopy is the lack of sample preparation; this greatly reduces the potential of user contamination and unintended reaction byproducts. With the study of graphene and C_{60}, stock samples were acquired from ACS Materials and SES Research Inc. respectively. No sample preparation was applied to the previously mentioned samples save C_{60}. It was subjected to use on the Edwards AUTO 306 vapor deposition chamber for deposition onto silver coated microscopic slides that were cleaned using a Piranha solution to remove any residual organic matter. Both the silver coating and C_{60} deposition were approximately 70 Å in thickness each.

The doped graphene samples for CO_2 capture provided by Dr. Chen for study were subject to various solutions and treatments as seen in Figure 10.[22] First, the graphite starting material was oxidized to graphite oxide. The graphite oxide was then exfoliated by ultrasound to graphene oxide. The final step was the functionalization of the graphene oxide by amine substitution with tetraethylenepentamine. It should also be noted that other hyper branched amines could potentially perform the same function as TEPA.

The doped biochar samples for heavy metal adsorption provided by Dr. Chen and Dr. Baharak Sajjadi were first treated with ultrasound to adjust the surface area and overall porosity of the sample then functionalized with urea using phosphoric acid.

The doped TiO_2 graphene samples provided by Dr. Nouranian varied in the amount of oxidation and titanium doping present per sample. They were studied based upon their oxidation state and the amount of GO present relative to TiO_2.

The samples for the SERSUN study were prepared by placing clean microscopic slides inside of a VDC where silver nanoparticles were deposited at approximately 70 Å thickness. Once the silver substrate had been deposited, a layer of C_{60} was deposited using the VDC again at a thickness of 70 Å. The coated slides were then treated to various physical treatments as seen in Figures 17 through 20.

3.2 Calibration

For the sake of consistent and precise measurements, the spectrometer was calibrated before every session to ensure proper spectral alignment using a silicon wafer chip placed on a microscopic slide. The two points of calibrations were at 0 and 520.6 cm^{-1}, indicating proper spectral alignment via a certified reference material unique to the individual spectrometer. It is also important to note that the laser wavelength and grating position were adjusted for calibration, not the camera or stage. In order to focus the sample in reference to the camera, it was necessary to adjust the stage vertically as the camera was placed above the stage and was stationary.

3.3 Measurements

For the majority of the samples studied, the YAG laser was used at a lower power setting. For solid samples, pre-cleaned microscopic glass slides were used. The sample was transferred to a slide via a double-ended micro-tapered stainless steel spatula from a clear or amber tinted cylindrical glass vial that had been stored out of direct sunlight in a wooden laboratory sample box. The samples were then gently spread by the broad side of the spatula to ensure that the macroscopic shape of the sample on the slide was flat in order to minimize shifts in optical focus of the camera while scanning the sample's local terrain. As has previously been shown in earlier research,[23] the focal length of the 100x objective lens was very sensitive to any vertical change. When studying samples of very sporadic physical form, locating a representative portion of the sample often proved challenging.

In theory, all of the samples under study were homogenous, however it was apparent that the resultant spectra was very much dependent on the location of laser placement for the sample under study. While changes in the fundamental vibrational frequencies Raman peaks were an exceptionally rare occurrence when studying different portions of the same sample, it was common to see an increase in noise or fluorescence from one portion of the sample under study to the next. It is quite plausible that the microscopic terrain of the sample had a large influence on the resultant Raman spectra. To better illustrate this point please see Figure 5 below.

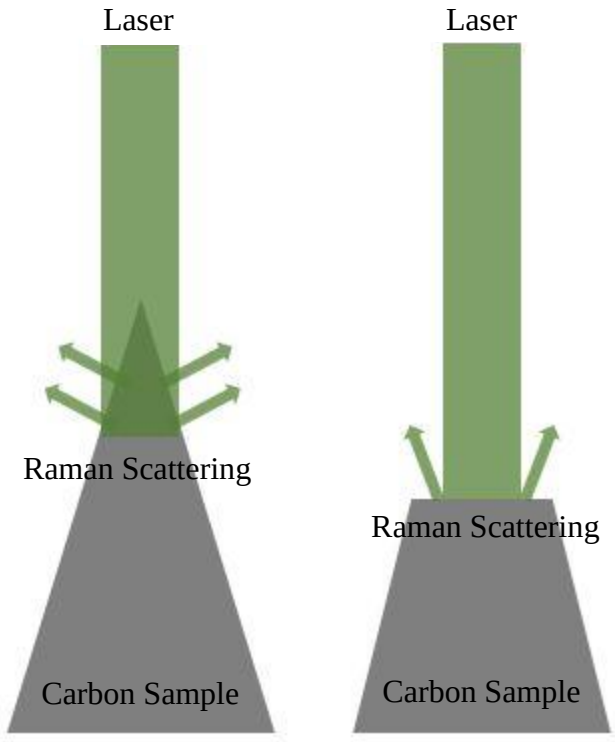

Figure 5 Microscopic Terrain: Depending on the elevation of the sample above the local microscopic terrain, it is found that the flatter sample mounds produce the best spectrum. As shown with the arrows, the angle of scattering is influenced by the angle of the surface with respect to the laser path.

Although difficult to illustrate or explain on paper, it is easiest to imagine the microscopic terrain as a mountainous landscape and the camera is a satellite directly above the mountain range. When scanning the sample with the camera, one will often see mounds or clumps of dark, dull carbon in the solid form. Given that the laser has a physical diameter of approximately 17 micrometers when using the 100x objective lens, it is quite plausible that the peak will not have as large of a cross sectional area as the laser. When such conditions are met, the sides of the peak are struck with the laser; this is usually the first indication of a poor resultant spectrum. It is theorized that the slope of

the sample surface directly affected the direction in which the light was scattered; with the majority of the scattered light not reaching the objective lens and hence the detector, a decrease in the signal to noise ratio ensued. This spectral event is not often mentioned in textbooks or research papers if ever, but it was continually a concern for my research efforts.

Another concern is the optical focus of the objective lens on the sample. In order to adjust the optical focus, the stage on which the microscopic slide rests is adjusted vertically and horizontally while the camera and objective lens remain stationary; the stage was able to move along three axes. For spectral measurements that take less than one half hour, there is little worry that the sample will become out of focus. However, if the spectrometer is used for longer than one hour on a single portion of the sample, there is a noticeable loss of optical focus due to the gradual mechanical falling of the stage due to non-locking gears. This is not a concern for the majority of researchers using the spectrometer, yet should be noted.

Chapter 4 Results

4.1 Graphene

As mentioned in earlier chapters of this text, understanding the theory behind the spectral peaks and relative intensities will allow for more accurate interpretation of the results. Given that graphene is a two-dimensional material, it can be easily described as a carbon film. Within pristine graphene films, the vast majority of carbons are sp^2 bonded. As such, the visible excitation of the laser will resonate with the π states of the six membered carbon rings of the lattice. When considering the entire molecular lattice, assigning the peaks should be straightforward.[24] The D peak at approximately 1350 cm^{-1} corresponds to the out of plane A_{1g} vibrational mode and can be structurally explained by the amount of defects in the graphene sheet and at the edge of the graphene film. The G peak at approximately 1580 cm^{-1} corresponds to the primary in-plane E_{2g} vibrational mode and is structurally explained by the stretching of the C-C bond in the graphene rings; it is common to all sp^2 carbon systems. The 2D peak at approximately 2850 cm^{-1} corresponds to the a second-order overtone of a different in-plane vibration of the D peak and is described structurally as the splitting of electron bands.[25] Of particular importance when comparing of various graphene-like materials as seen in Figures 6 through 9, it is useful to compare the relative peak intensities of the D and G peaks as the I_D/I_G ratio.

This ratio is largely indicative of the relative amount of structural defects in the graphene sheets.

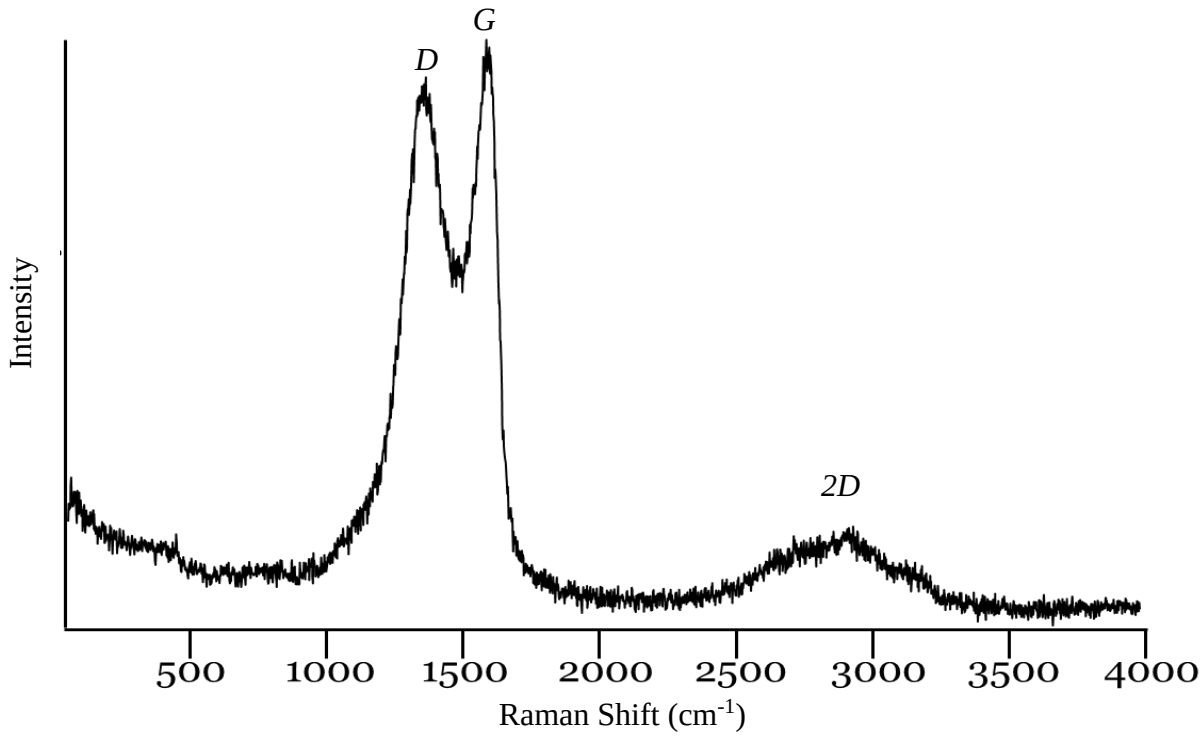

Figure 6 Graphene Powder Raman: The above spectrum was the first data I had collected from the Raman spectrometer. The *D, G,* and *2D* peaks are seen from lower to high wavenumbers respectively. The powder was obtained from ACS Materials.

The Raman spectrum of Micro 450, Micro 850, and Micro 4827 are useful in illustrating the spectral effects that varying physical properties have. Micro 450 is a synthetic carbon flake with a particle size ranging from 3 to 7 µm with an average of approximately 5 µm. Micro 850 is a natural carbon flake with a particle size ranging from 3 to 5 µm with an average size of approximately 5 µm. Micro 4827 is a surface enhanced synthetic carbon flake with a nominal size of 2 µm. While Micro 450 and Micro 850 have a similar surface area of 17 and 14 m^2/gram, Micro 4827 has a surface area of 113 m^2/gram.

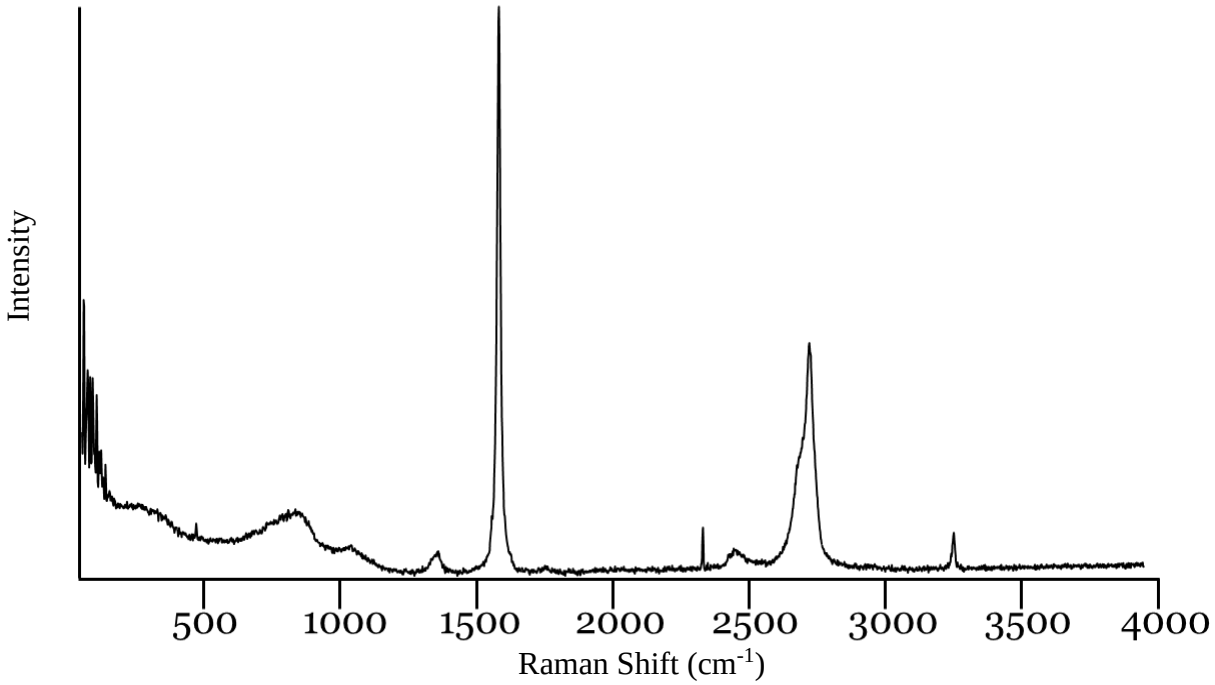

Figure 7 Graphite Raman: The above spectrum of graphite flakes is useful in illustrating the I_D/I_G ratio found in graphene-like samples. When examining the spectrum of graphite in comparison to graphene, it is useful to note the "hump" that occurs in the 2D peak is sectioned into $2D_1$ and $2D_2$ which occur at lower and higher wavenumbers respectiveley.[26]

While numerous variable exist that might explain the differences in the I_D/I_G ratio, one of the most obvious is the surface area of the samples.[27] Given that the I_D/I_G ratio increased from Micro 850 to Micro 450 then to Micro 4827, one can summarize that as the surface area of the flakes increased the measure of structural disorder increases. Given that the project was ultimately attempting to use a graphene-like substrate to attach functional groups onto for CO_2 capture, the logical choose was to reduce Micro 850 based on its low I_D/I_G ratio to graphene oxide. Once reduced to graphene oxide, the sample was subjected to TEPA in solution by two potential routes to transfer amine groups to the graphene oxide.[28] The first method involves N-hydroxysuccinimide in the

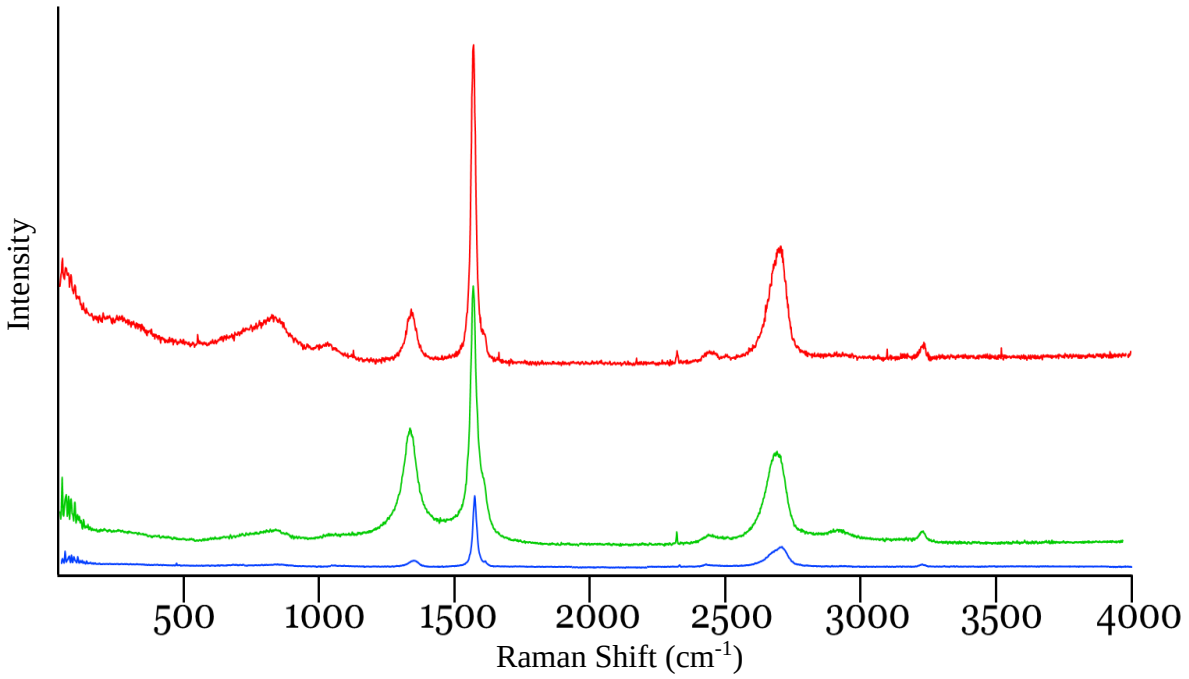

Figure 8 Micro 450, Micro 850, and Micro 4827 Raman: The above graph combines the Raman spectra of Micro 450 (red, top), Micro 850 (blue, bottom), and Micro 4827 (green, middle). The I_D/I_G ratio of the samples are as follows: 0.204, 0.156, and 0.481 respectively. The I_{2D}/I_G ratios of the samples are as follows: 0.403, 0.338, and 0.396 respectively. Note that these measurements were done using the peak intensity and not the integrated area under the peak.

presence of 1-ethyl-3-(3-dimethylaminopropyl)carbodiimide. The second method involves a reflux of KOH and water at 80 ℃.

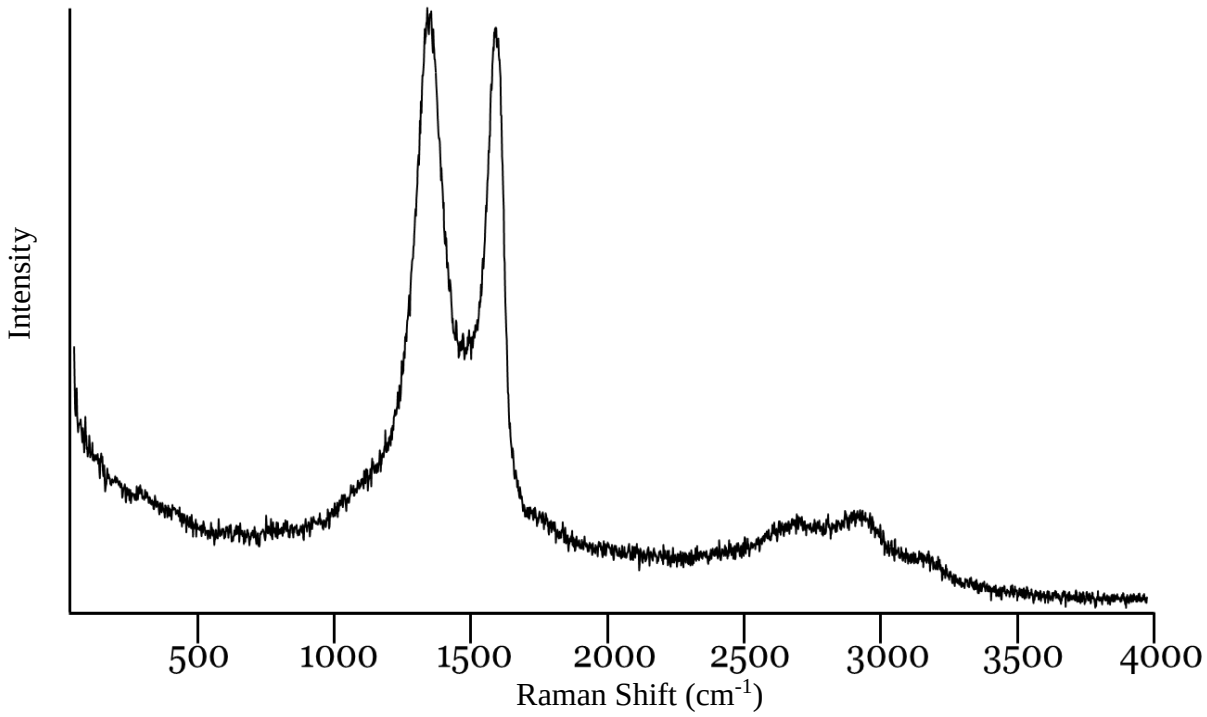

Figure 9 GO Raman: The above spectrum represents the Raman spectrum of GO provided by Dr. Chen using a 532 nm laser.

4.2 Doped Biochar and Graphene

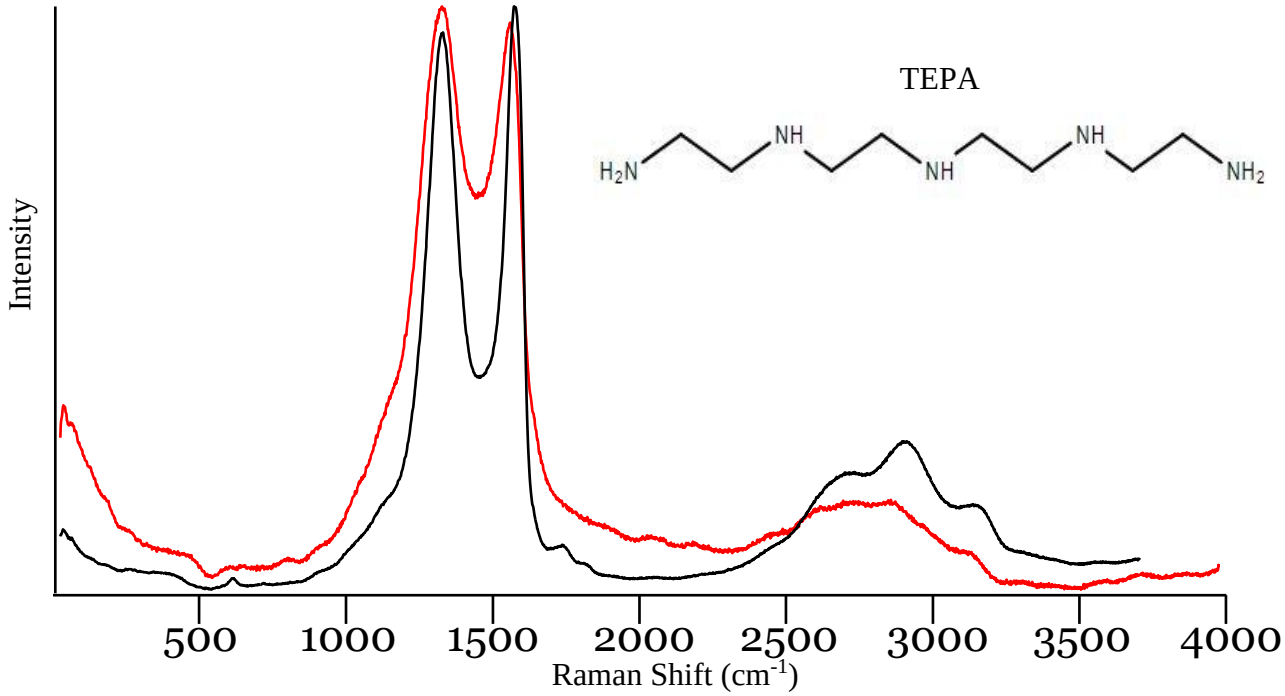

Figure 10 GO-TEPA and GO: The black line represents GO. The red line represents the attempt of adding TEPA[29] functional groups via microwaves to the GO. At the D and G peaks of GO-TEPA, red shift of 3 cm^{-1} and 15 cm^{-1} are seen respectively. Also, the I_D/I_G ratio calculated using the integrated area under the peak changed from 1.42 to 1.38 for GO to GO-TEPA.

When comparing this experimental results to previous works,[30] it is clear that a shift does occur in the I_D/I_G ratio when TEPA functional groups replace the epoxy, carboxyl, and hydroxyl groups of GO. When comparing directly between GO and GO-TEPA, previous works show an increase in the I_D/I_G ratio; this was not the case in our experimental results as the ratio slightly decreased. The anticipated increase is theorized to occur due an increase of defects in the graphene sheets, functional group substitution,

and increase in the number of sp^3 bonded carbons. Also, shifts in the D and G band were noted. When comparing GO and GO-TEPA, a blue shift of 15 cm^{-1} was noted for the D peak and 3 cm^{-1} for the G peak. The shifts likely indicate the presence of electron withdrawing groups, especially in the G peak. The overall intensity of the 2D peak is decreased in the GO-TEPA as seen in previous work. With the conflicting nature of the results presented in comparison to previous work, a clear conclusion regarding the presence of nitrogen containing functional groups on GO cannot be made with confidence from the results presented.

Despite the ambiguity in the conclusions drawn from the spectral results of the graphene functionalized with the amine groups of TEPA, the experiment was revised to use biochar and functionalize it by using ultrasound, phosphoric acid, and urea as demonstrated in Figures 11 through 13.[31]

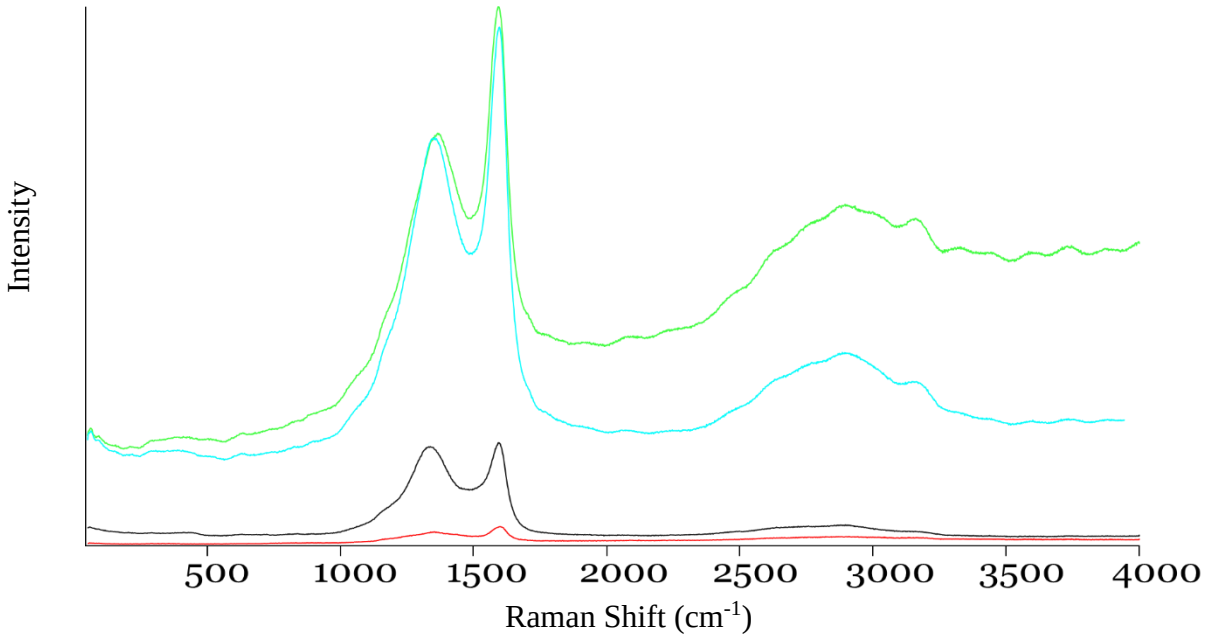

Figure 11 Biochar and Different Ultrasound Durations: The spectra of US0-P50%-UR6M, US20-P50%-UR6M, US40-P50%-UR6M, and raw biochar are labeled as red, black, blue, and green lines respectively. The I_D/I_G ratio were calculated as 0.749, 0.96, 0.78, and 0.766 respectively.

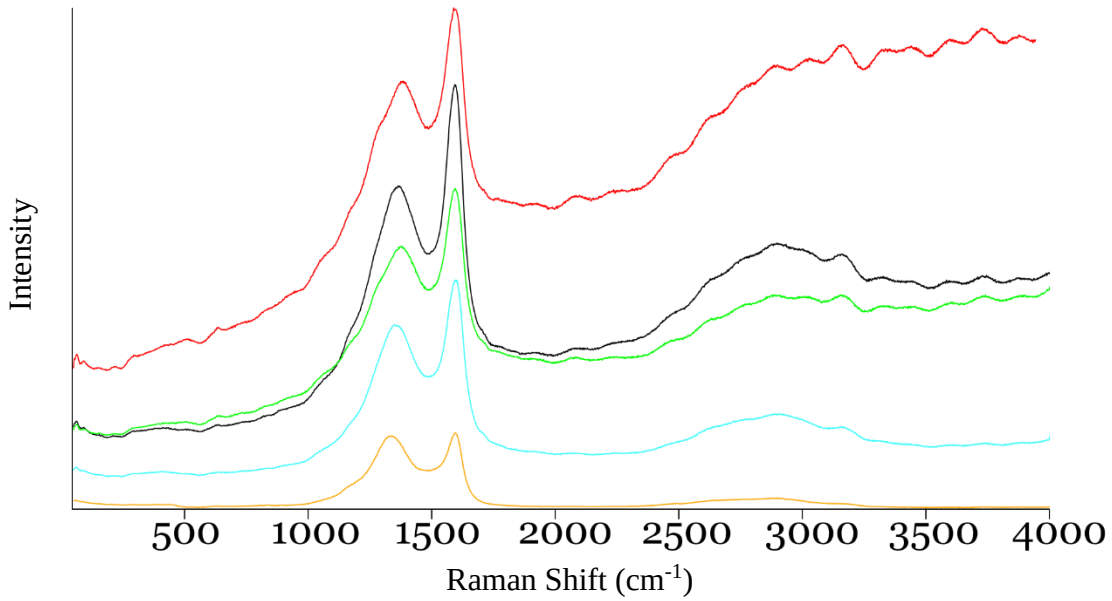

Figure 12 Biochar and Different Phosphoric Acid Concentrations: The spectra of US20-P0%-UR6M, US20-P25%-UR6M, US20-P50%-UR6M, US20-P85%-UR6M, and raw biochar are labeled as red, orange, green, blue, and black lines respectively. The I_D/I_G ratio were calculated as 0.813, 0.825, 0.963, 0.856, and 0.766 respectively.

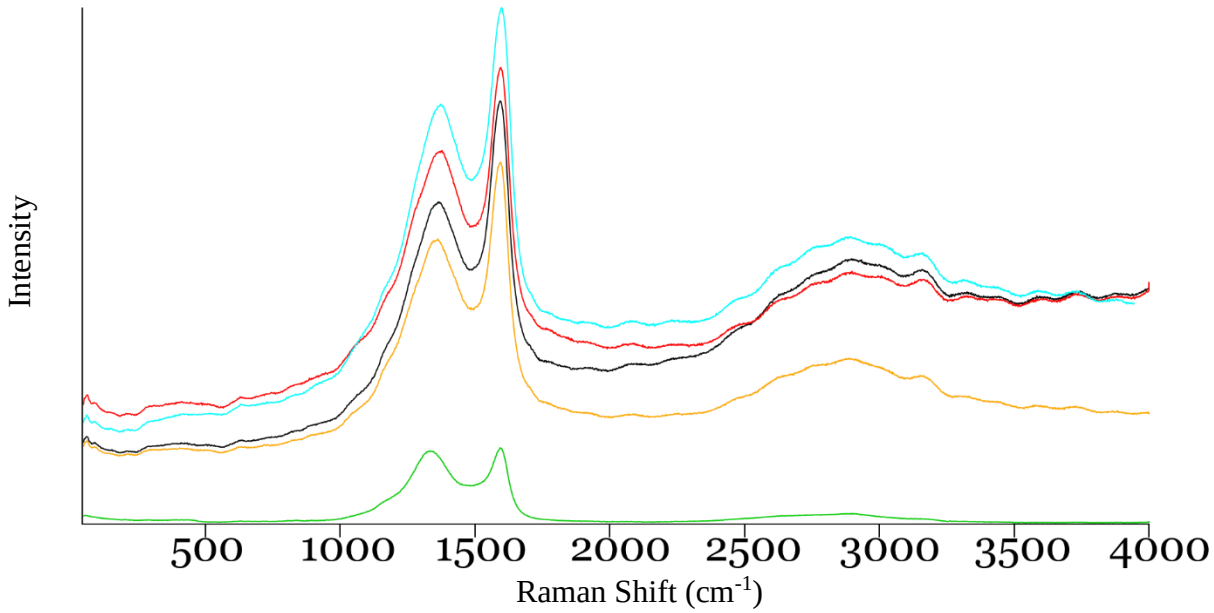

Figure 13 Biochar and Different Urea Concentrations: The spectra of US20-P50%-UR1M, US20-P50%-UR3M, US20-P50%-UR6M, US20-P50%-UR10M, and raw biochar are labeled as red, orange, green, blue, and black lines respectively. The I_D/I_G ratio were calculated as 0.821, 0.793, 0.963, 0.816 and 0.766 respectively.

When collaborating with Dr. Nouranian, the objective now became to investigate the effects of substrate chemistry and TiO_2/GO ratios as seen in Figures 14 through 16 on the grafting and distribution of graphene layers on TiO_2. While the photocatalytic activity of the composite will eventually be measured, the data is not yet complete and as such the following graphs are preliminary results of the spectroscopic portion of the study. As of yet, published literature have compared the I_D/I_G ratio amongst samples[32] but have not compared the relative intensities of the D and G peak to the titanium peak at approximately 150 cm^{-1}.

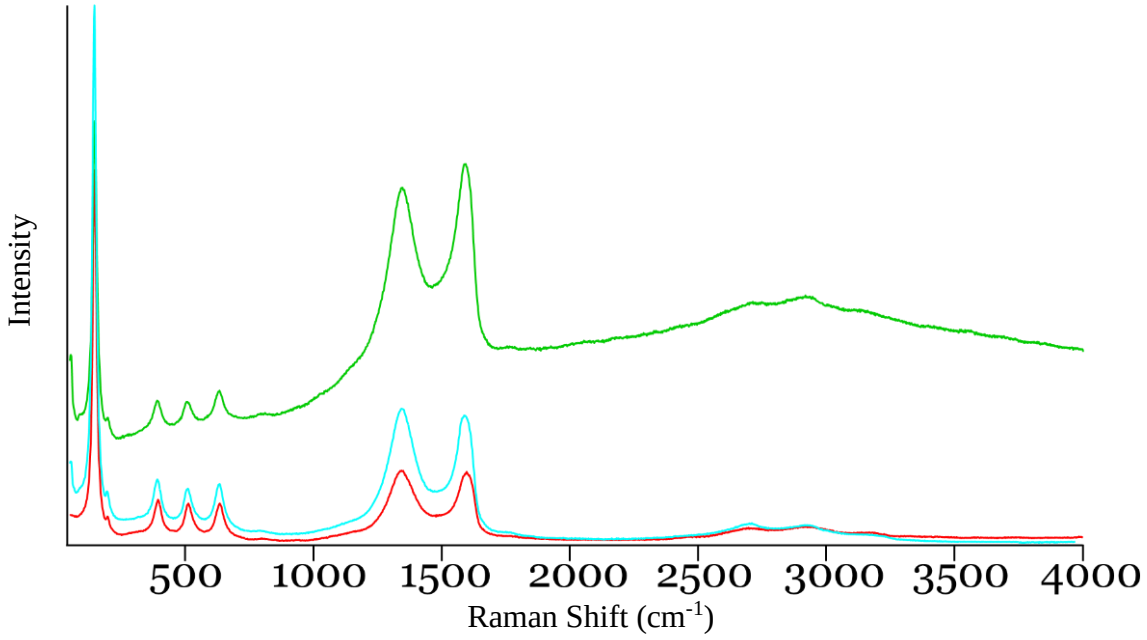

Figure 14 GO-TiO_2 Low Oxidation: The graph above is represented by GO-TiO_2 at low oxidation levels. The red, green, and blue line represent the GO-TiO_2 low oxidation levels at 5%, 10%, and 20% GO to TiO_2. The I_D/I_G ratio was calculated to be 1.01, 0.94, and 1.04 respectively by relative peak height.

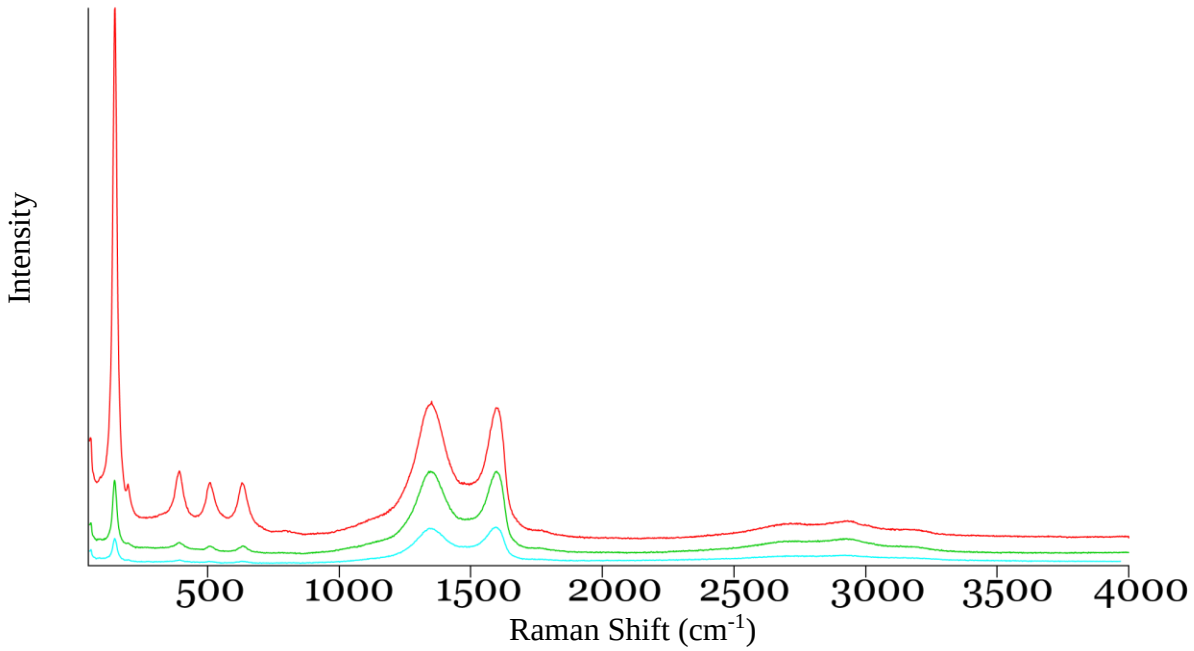

Figure 15 GO-TiO_2 Mid Oxidation: The graph above is represented by GO-TiO_2 at mid oxidation levels. The red, green, and blue line represent the GO-TiO_2 mid oxidation levels at 5%, 10%, and 20% GO to TiO_2. The I_D/I_G ratio was calculated to be 1.04, 1.00, and 0.97 respectively by relative peak height.

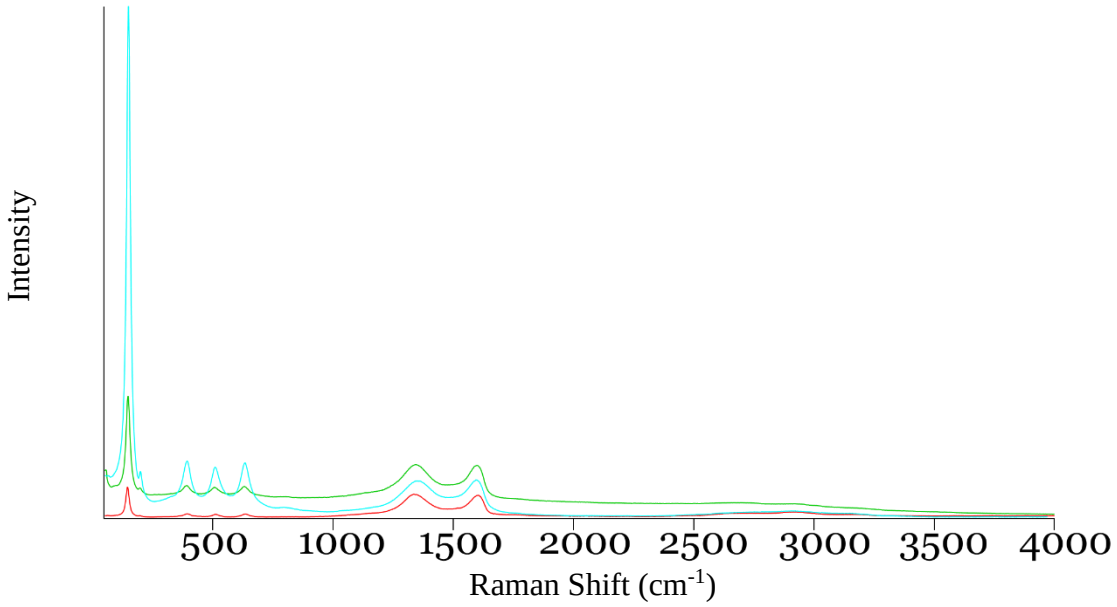

Figure 16 GO-TiO_2 High Oxidation: The graph above is represented by GO-TiO_2 at high oxidation levels. The red, green, and blue line represent the GO-TiO_2 high oxidation levels at 5%, 10%, and 20% GO to TiO_2. The I_D/I_G ratio was calculated to be 1.03, 1.01, and 0.97 respectively by relative peak height.

4.3 SERSUN

As previously mentioned in the preceeding text, a novel Raman enhancement technique was attempted involving SERS and RUNS in combination as SERSUN. The following Table 1 lists the fundamental Raman frequencies and symmetries of C_{60}. Figures 17 through 20 display the Raman spectra of various stages of the experiment as it progressed.

Table 1: Raman Frequencies and Symmetries of C_{60}*:* The above table represents the ten fundamental vibration frequencies and Raman active modes of C_{60}.[33]

273 cm^{-1}	437 cm^{-1}	496 cm^{-1}	710 cm^{-1}	774 cm^{-1}
H_g (1)	H_g (2)	A_g (1)	H_g (3)	H_g (4)
1099 cm^{-1}	1250 cm^{-1}	1428 cm^{-1}	1470 cm^{-1}	1575 cm^{-1}
H_g (5)	H_g (6)	H_g (7)	A_g (2)	H_g (8)

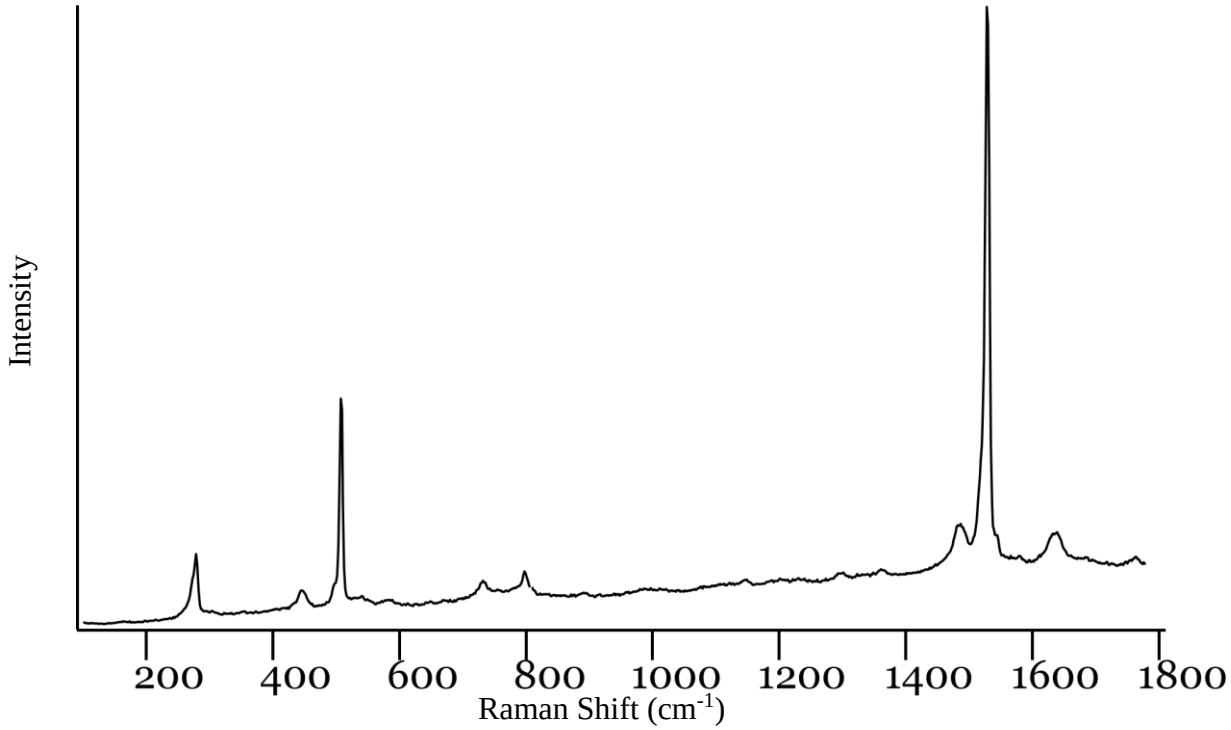

Figure 17 C_{60} *Powder Raman:* The above spectrum was gathered using a 532 nm laser. The experiment was conducted under atmospheric conditions and ambient laboratory temperatures. A microscopic slide with no coating was placed under the sample.

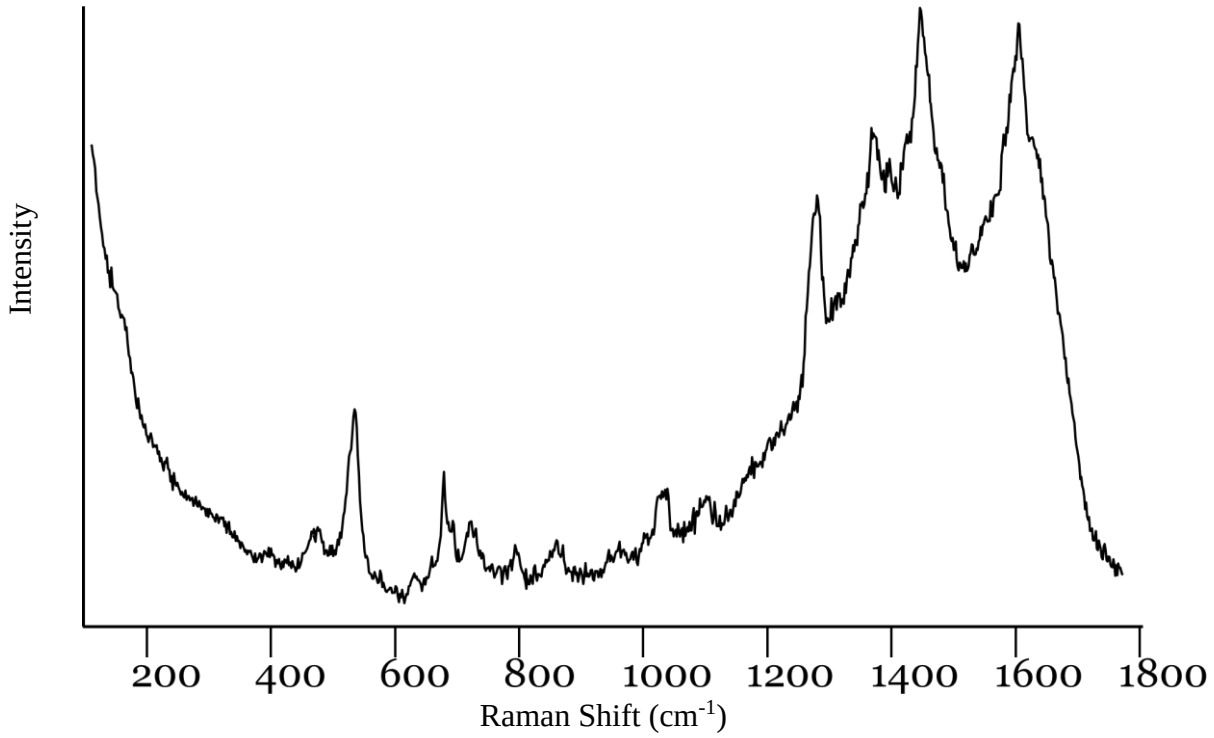

Figure 18 SERS of C_{60}*:* Based on the overall shape of the spectrum, it is obvious that the silver coated slides not did improve the signal to noise ratio of the C_{60} experiment when compared to non-treated slides. This experiment occurred at atmospheric conditions and ambient laboratory temperatures.

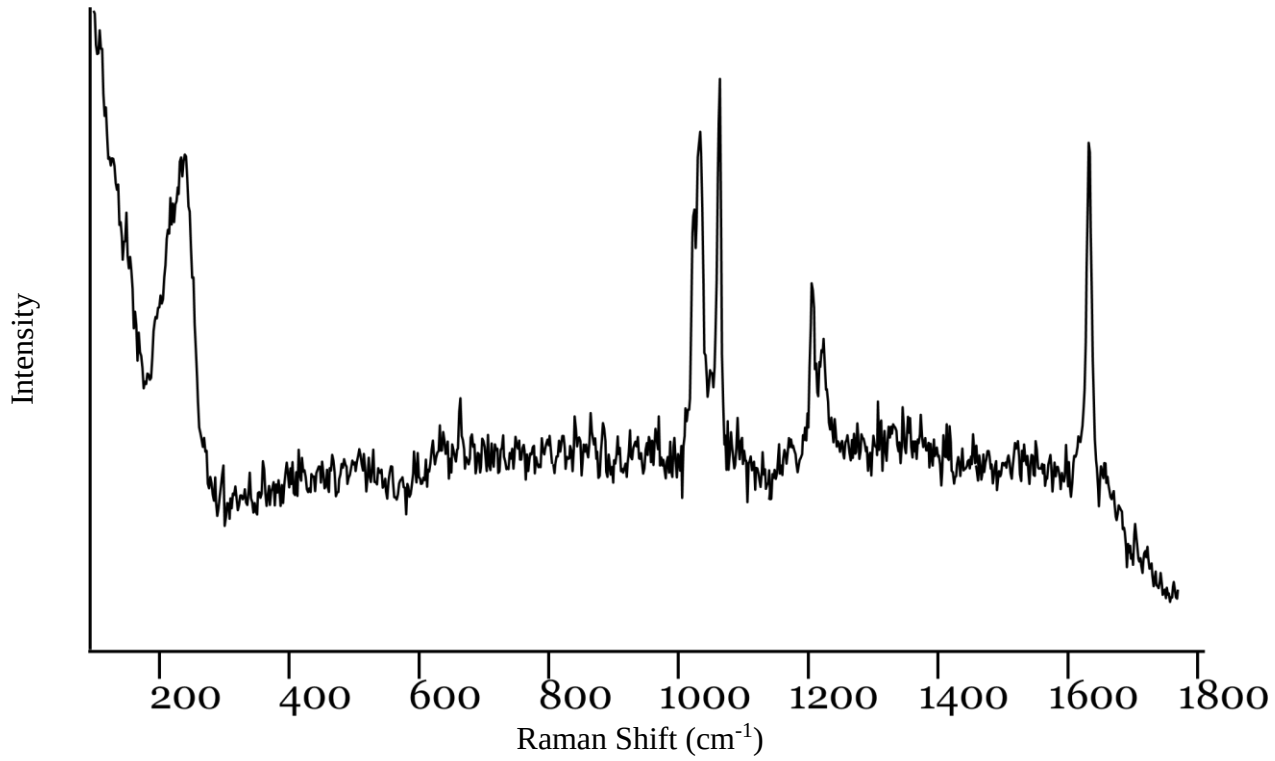

Figure 19 SERS of C_{60} *at Reduced Temperatures:* When compared to the SERS spectra at ambient temperatures, some of the spectral features are seen to diminish; specifically the fluorescence that occurs past 1000 wavenumbers. This is most likely explained by the reduced temperatures (123 K) of the study.

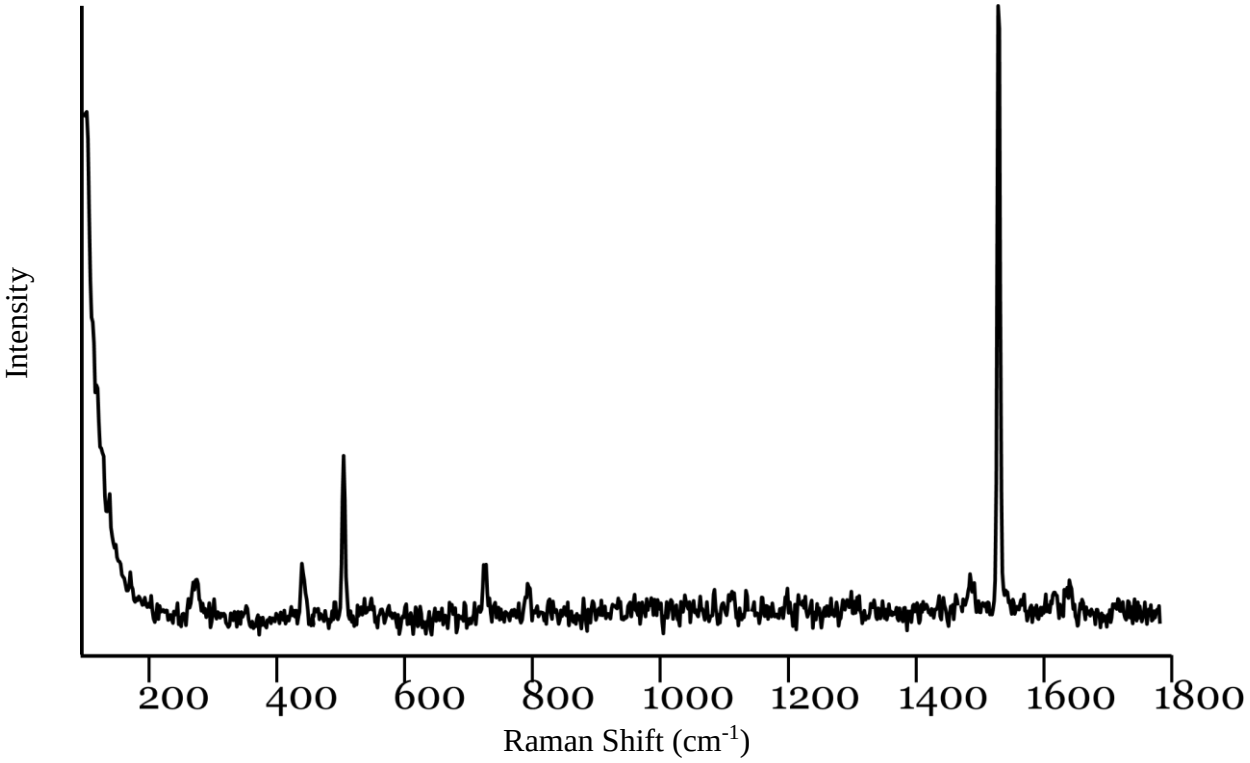

Figure 20 RUNS of C_{60}*:* When loose powder samples were submerged under liquid nitrogen in a porcelain bowl, the signal to noise ratio was greatly increased. Note that the sample was placed at the bottom of the bowl with no treated slide placed underneath the sample.

Chapter 5 Conclusions

5.1 Graphene

Although simple and straightforward in theory, the opportunity to study graphene and derivatives was very rewarding for a number of reasons. First, I was able to become accustomed to the working of the spectrometer and how it operates. Second, interpreting the data collected proved valuable in future work as the spectra became more complex and less indicative. Third, I became more confident in my ability to overcome difficulties as they arose during experiments. It should also be noted that many locations on the sample were measured before a representative spectra was saved as data.

5.2 Doped Biochar and Graphene

When studying the effects of sample preparation, it is imperative that all experimental parameters remain constant in order to eliminate the potential for skewed results. As such, great care was taken to ensure that the samples were measured in the same manner. Therefore, the resultant spectra can be used at face value with no data corrections necessary.

With respect to the doped graphene provided by Dr. Chen, the resultant Raman spectrum of GO-TEPA was not definitive enough to give a conclusive answer on whether the GO was indeed functionalized with nitrogen containing functional groups.

With respect to the doped biochar provided by Dr. Chen and Dr. Sajjadi, the Raman results clearly show that the biochar was indeed functionalized. Although not clear from the spectra, it was later shown that the modified biochar was able to remove significantly more heavy metals than raw biochar.[31]

With respect to the GO-TiO_2, further study is needed to reach a definitive conclusion. However, when comparing the results amongst their oxidation tiers, interesting trends seem to appear but more data is need to make a definitive statement regarding the preliminary trends.

5.3 SERSUN

Attempting to perform a novel method of Raman enhancement proved to be a more difficult task than anticipated. In theory, one would expect that the SERS portion of the experiment would be nicely complimented when submerged under liquid nitrogen to mitigate the effects of sample degradation when more laser power is desired to increase the signal to noise ratio.

In order for SERS to be an effective method of Raman enhancement, the localized surface plasmons excited at the silver-C_{60} interface must amplify the electromagnetic fields. Given that the experiment should have produced very impressive results in theory, it is likely that a mistake was made in the experimental procedure. In retrospect, the most

likely step for error was the VDC; no validation of the silver or graphene deposition was made save the balance arm inside the chamber.

Chapter 6 Future Work

Although ultimately unsuccessful, the intentions behind the SERSUN method of Raman enhancement should not be discredited. The potential uses of further research using these methods are largely unknown. Given that both methods have found favor with researchers in the Hammer Research Group and abroad, a combination of the methods makes theoretical and logistical sense. The only portion lacking is the exact experimental setup that would allow for the coated slide to be submerged in liquid nitrogen at a shallow enough depth to minimize interference from the gas bubbling as the slide temperature equates to the temperature of liquid nitrogen (77 K). In theory, one would simply pre-cool the slide before submersion into the bowl of liquid nitrogen or continuously add liquid nitrogen as it boils off, yet both in principle are hard to achieve. First, if one were able to chill the slide to the point of 77 K, it is unlikely that the transfer from refrigerator to bowl would occur without a marked increase in temperature of the slide from the ambient room atmosphere due to the high surface area of the slide and high thermal conductivity. Second, adding liquid nitrogen usually causes intensification in the boiling of the liquid nitrogen.

Given that the problem exists in the RUNS portion of the experiment and not the SERS portion, the logical solution would be to eliminate the need for submersion into liquid nitrogen and instead use a temperature controlled study. In our laboratory, a Linkam Scientific THMS600 Temperature Controlled Stage is available for use and has been used with successful results in previous studies in which local heating of the sample was degrading the sample. Although my individual results were only slightly better than

SERSUN, it is again suggested that the method not be immediately dismissed for similar reasons as stated above.

List of References

1. Krishnan, R. S., and R. K. Shankar. "Raman Effect: History of the Discovery." *Journal of Raman Spectroscopy* 10, no. 1 (1981): 1-8.

2. Baer, Thomas M., and Mark S. Keirstead. "Nd-YAG laser." U.S. Patent 4,653,056, issued March 24, 1987.

3. Ferraro, John R. *Introductory Raman Spectroscopy*. Academic Press, 2003**:** 22

4. *CamGraph® Graphene Powder*; MSDS [Online]; Cambridge Nanosystems Ltd: Cambridge UK, May, 2018. https://cambridgenanosystems.com (accessed April 10, 2018).

5. Engel, Thomas, and Philip Reid. *Physical Chemistry*. 3rd ed. Boston, MA: Pearson, 2013.

6. Raman, Chandrasekhara V. "A Change of Wave-length in Light Scattering." *Nature* 121, no. 3051 (1928): 619.

7. Rasetti, F. "Raman Effect in Gases." *Nature* 123, no. 3093 (1929): 205.

8. Pence, Isaac, and Anita Mahadevan-Jansen. "Clinical Instrumentation and Applications of Raman Spectroscopy." *Chemical Society Reviews* 45, no. 7 (2016): 1958-1979.

9. Yu, Guanglin, Yan Rou Yap, Kathryn Pollock, and Allison Hubel. "Characterizing Intracellular Ice Formation of Lymphoblasts Using Low-Temperature Raman Spectroscopy." *Biophysical Journal* 112, no. 12 (2017): 2653-2663.

10. Kudelski, Andrzej. "Analytical Applications of Raman Spectroscopy." *Talanta* 76, no. 1 (2008): 1-8.

11. Verma, Prabhat. "Tip-Enhanced Raman Spectroscopy: Technique and Recent Advances." *Chemical Reviews 117* (9) , (2017): 6447-6466

12. Compton, R. N., and N. I. Hammer. "Raman Under Liquid Nitrogen (RUN)." In *Journal of Physics: Conference Series*, vol. 548, no. 1, p. 012017. IOP Publishing, 2014.

13. Hager, J. Stewart, James Zahardis, Richard M. Pagni, Robert N. Compton, and Jun Li. "Raman Under Nitrogen. The High-Resolution Raman Spectroscopy of Crystalline Uranocene, Thorocene, and Ferrocene." *The Journal of Chemical Physics*120, no. 6 (2004): 2708-2718.

14. Larkin, Peter. *Infrared and Raman Spectroscopy: Principles and Spectral Interpretation*. Elsevier, 2017.

15. Novoselov, Kostya S., Andre K. Geim, Sergei V. Morozov, D. Jiang, Y_ Zhang, Sergey V. Dubonos, Irina V. Grigorieva, and Alexandr A. Firsov. "Electric Field Effect in Atomically Thin Carbon Films." *Science* 306, no. 5696 (2004): 666-669.

16. Boehm, Hans-Peter, A. Clauss, G. O. Fischer, and U. Hofmann. "Das Adsorptionsverhalten Sehr Dünner Kohlenstoff-folien." Zeitschrift Für Anorganische und Allgemeine Chemie 316, no. 3-4 (1962): 119-127.

17. Lee, Jae-Hwang, David Veysset, Jonathan P. Singer, Markus Retsch, Gagan Saini, Thomas Pezeril, Keith A. Nelson, and Edwin L. Thomas. "High Strain Rate Deformation of Layered Nanocomposites." *Nature Communications* 3 (2012): 1164.

18. Moradi, Omid, Vinod Kumar Gupta, Shilpi Agarwal, Inderjeet Tyagi, Mohammad Asif, Abdel Salam Hamdy Makhlouf, Hamidreza Sadegh, and Ramin Shahryari-ghoshekandi. "Characteristics and Electrical Conductivity of Graphene and Graphene Oxide for Adsorption of Cationic Dyes from Liquids: Kinetic and Thermodynamic Study." *Journal of Industrial and Engineering Chemistry* 28 (2015): 294-301.

19. Falkovsky, L. A. "Optical Properties of Graphene." In *Journal of Physics: Conference Series*, vol. 129, no. 1, p. 012004. IOP Publishing, 2008.

20. Qu, Liangti, Yong Liu, Jong-Beom Baek, and Liming Dai. "Nitrogen-Doped Graphene as Efficient Metal-Free Electrocatalyst for Oxygen Reduction in Fuel Cells." *ACS Nano* 4, no. 3 (2010): 1321-1326.

21. Kroto, H. W., J. R. Heath, S. C. O'brien, R. F. Curl, and R. E. C. Smalley. "This Week's Citation Classic®." *Nature* 318 (1985): 162-163.

22. Chatterjee, Riya, Baharak Sajjadi, Daniell L. Mattern, Wei-Yin Chen, Tetiana Zubatiuk, Danuta Leszczynska, Jerzy Leszczynski, Nosa O. Egiebor, and Nathan Hammer. "Ultrasound Cavitation Intensified Amine Functionalization: A Feasible Strategy for Enhancing CO_2 Capture Capacity of Biochar." *Fuel* 225 (2018): 287-298.

23. Tsang, Lemuel S. Raman Spectroscopic Studies of Novel Gold-Containing Nanomaterials. Undergraduate's thesis, University of Mississippi, 2017: 16-17.

24. Malard, L. M., M. A. A. Pimenta, G. Dresselhaus, and M. S. Dresselhaus. "Raman Spectroscopy in Graphene." Physics Reports 473, no. 5-6 (2009): 51-87.

25. Childres, Isaac, Luis A. Jauregui, Wonjun Park, Helin Cao, and Yong P. Chen. "Raman Spectroscopy of Graphene and Related Materials." *New Developments in Photon and Materials Research* 1 (2013).

26. Ferrari, Andrea C. "Raman Spectroscopy of Graphene and Graphite: Disorder, Electron–Phonon Coupling, Doping and Nonadiabatic Effects." *Solid State Communications* 143, no. 1-2 (2007): 47-57.

27. "Graphite and Carbon Powders for Grease and Lubricant Manufactures." August 1, 2016. Accessed April 10, 2018. asbury.com.

28. Chen, Wei-Yin, and Daniell L. Mattern. "Interactions between Char and CO_2 - to Create a Cradle-to-Cradle Carbon Cycle, and , - to Develop Advanced Sorbents for Carbon Capture." Lecture, University of Mississippi.

29. "TEPA." *National Center for Biotechnology Information. PubChem Compound Database*, U.S. National Library of Medicine, pubchem.ncbi.nlm.nih.gov/compound/tepa#section=Top. Accessed 12 Apr. 2018.

30. Ribeiro, Helio, Wellington Marcos da Silva, Juliana Cardoso Neves, Hállen Daniel Resende Calado, Roberto Paniago, Luciana Moreira Seara, Denise das Mercês Camarano, and Glaura Goulart Silva. "Multifunctional Nanocomposites Based on Tetraethylenepentamine-Modified Graphene Oxide/Epoxy." *Polymer Testing* 43 (2015): 182-192.

31. Sajjadi, Baharak, James W. Broome, Wei-Yin Chen, Daniell Mattern, Nosa O. Egiebor, Nathan Hammer, and Cameron L. Smith. "Urea Functionalization of Ultrasound-Treated Biochar: A Feasible Strategy for Enhancing Heavy Metal Adsorption Capacity." *Ultrasonics Sonochemistry*.

32. Bethune, Donald S., Gerard Meijer, Wade C. Tang, and Hal J. Rosen. "The Vibrational Raman Spectra of Purified Solid Films of C_{60} and C_{70}." *Chemical Physics Letters* 174, no. 3-4 (1990): 219-222.

33. Kamegawa, Takashi, Daiki Yamahana, and Hiromi Yamashita. "Graphene Coating of TiO_2 Nanoparticles Loaded on Mesoporous Silica for Enhancement of Photocatalytic Activity." *The Journal of Physical Chemistry C* 114, no. 35 (2010): 15049-15053.